J|A|C|S
ARTICLES
Published on Web 03/30/2002

Theoretical Studies To Understand Surface Chemistry on Carbon Anodes for Lithium-Ion Batteries: How Does Vinylene Carbonate Play Its Role as an Electrolyte Additive?

Yixuan Wang,*,† Shinichiro Nakamura,‡ Ken Tasaki,§ and Perla B. Balbuena*,†

Contribution from the Department of Chemical Engineering, Swearingen Engineering Center, University of South Carolina, Columbia, South Carolina 29208, Mitsubishi Chemical Corporation, MCC-Group Science and Technology Research Center, 1000 Kamoshida-cho, Aoba-ku, Yokohama 227-8502, Japan, and MC Research and Innovation Center, Mountain View, California 94041

Received September 13, 2001

Abstract: To elucidate the role of vinylene carbonate (VC) as a solvent additive in organic polar solutions for lithium-ion batteries, reductive decompositions for vinylene carbonate (VC) and ethylene carbonate (EC) molecules have been comprehensively investigated both in the gas phase and in solution by means of density functional theory calculations. The salt and solvent effects are incorporated with the clusters $(EC)_nLi^+(VC)$ ($n = 0-3$), and further corrections that account for bulk solvent effects are added using the polarized continuum model (PCM). The electron affinities of $(EC)_nLi^+(VC)$ ($n = 0-3$) monotonically decrease when the number of EC molecules increases; a sharp decrease of about 20.0 kcal/mol is found from $n =$ 0 to 1 and a more gentle variation for $n > 1$. For $(EC)_nLi^+(VC)$ ($n = 1-3$), the reduction of VC brings about more stable ion-pair intermediates than those due to reduction of the EC molecule by 3.1, 6.1, and 5.3 kcal/mol, respectively. This finding qualitatively agrees with the experimental fact that the reduction potential of VC in the presence of Li salt is more negative than that of EC. The calculated reduction potentials corresponding to radical anion formation are close to the experimental potentials determined with cyclic voltammetry on a gold electrode surface (−2.67, −3.19 eV on the physical scale for VC and EC respectively vs experimental values −2.96 and −2.94 eV). Regarding the decomposition mechanisms, the VC and EC moieties undergo homolytic ring opening from their respective reduction intermediates, and the energy barrier of VC is about one time higher than that of EC (e.g., 20.1 vs 8.8 kcal/mol for $(EC)_2Li^+(VC)$); both are weakly affected by the explicit solvent molecules and by a bulk solvent represented by a continuum model. Alternatively, starting from the VC-reduction intermediate, the ring opening of the EC moiety via an intramolecular electron-transfer transition state has also been located; its barrier lies between those of EC and VC (e.g., 17.2 kcal/mol for $(EC)_2Li^+(VC)$). On the basis of these results, we suggest the following explanation about the role that VC may play as additive in EC-based lithium-ion battery electrolytes; VC is initially reduced to a more stable intermediate than that from EC reduction. One possibility then is that the reduced VC decomposes to form a radical anion via a barrier of about 20 kcal/mol, which undergoes a series of reactions to give rise to more active film-forming products than those resulting from EC reduction, such as lithium divinylene dicarbonate, Li−C carbides, lithium vinylene dicarbonate, R−O−Li compound, and even oligomers with repeated vinylene and carbonate-vinylene units. Another possibility starting from the VC-reduction intermediate is that the ring opening occurs on the unreduced EC moiety instead of being on the reduced VC, via an intramolecular electron transfer transition state, the energy barrier of which is lower than that of the former, in which VC just helps the intermediate formation and is not consumed. The factors that determine the additive functioning mechanism are briefly discussed, and consequently a general rule for the selection of electrolyte additive is proposed.

Introduction

Lithium-ion batteries have become popular power sources for advanced portable electronics such as notebook computers and cellular phones because they provide a good combination of reversibility and high energy density; the relevant chemistry problems thereby have been attracting attention both from experimentalists and from theoreticians.[1,2] A typical lithium-ion battery system is made up of a graphite anode, a nonaqueous organic electrolyte that acts as an ionic path between electrodes and separates the two electrode materials, and a transition metal oxide (such as $LiMn_2O_4$, $LiCoO_2$) cathode. The most usual

* To whom correspondence should be addressed. E-mail: Y.W., wangyi@engr.sc.edu; P.B.B., balbuena@engr.sc.edu.
† University of South Carolina.
‡ Mitsubishi Chemical Corp.
§ MC Research and Innovation Center.

(1) Tarascon, J.-M.; Armand, M. *Nature* **2001**, *414*, 359−367.
(2) Armstrong, A. R.; Bruce, P. G. *Nature* **1996**, *381*, 499−500.

10.1021/ja017073i CCC: $22.00

electrolytes are the mixtures of alkyl carbonates, for example, ethylene carbonate (EC), propylene carbonate (PC), and lithium salts such as $LiAsF_6$ and $LiPF_6$. It is generally accepted that organic electrolytes are decomposed during the first lithium intercalation into graphite to form a solid electrolyte interface (SEI) film between the graphite anode surface and the electrolyte, and it is the SEI film that largely determines the performance of graphite as anode in rechargeable batteries.[3] For instance, the higher the film passivating ability, the better capacity and longer life cycle of the lithium-intercalated graphite anodes.

PC is an attractive solvent for nonaqueous-electrolyte batteries because of its superior ionic conductivity over a wide temperature range. However, PC electroreduction products do not properly passivate the graphite electrode;[4,5] that is, no effective SEI is formed on the graphite surface, and thus massive solvent molecules are reduced, and subsequent exfoliation on the graphite is observed. Consequently, there have been a lot of efforts to find proper additives to PC-based electrolytes, which help generate an effective SEI layer. Several additives have been reported, including chloroethylene carbonate (CEC), other halogen-substituted carbonates,[6] and a variety of unsaturated carbonates, such as vinylene carbonate (VC) and halogen substituted VC,[7] and ethylene sulfite (ES).[8] Often present in small amounts (5−10% volume), these additives, together with the solvents (PC, or mixtures of EC and PC, referred to as supporting solvent hereafter) could form the desirable protective interface. It seems therefore that the introduction of a proper additive to PC-based electrolyte is a very promising way to considerably improve the battery performance. However, there are very few experimental as well as theoretical studies about the mechanism by which these additives may act efficiently increasing the performance of lithium-ion batteries; the nature and the required amount of additives are therefore defined by costly trial-and-error experiments. The most fundamental question is what are the governing factors that make a species a good additive. Regarding the reaction mechanisms, questions to be answered include whether the SEI film directly comes from reduction products of the additives, or if the additives (reduction products or intermediates) just initiate a reduction process in which the main solvent is reduced and it becomes the active film-forming agent leading to the formation of more effective films comparable with the pure solvent, or if both mechanisms act simultaneously.

A rational search for a proper additive candidate demands a good understanding of the functioning mechanism of electrolyte additives, by which the governing factors could be determined from relevant aspects, such as the binding energy between lithium ion and additive/solvent, reduction potentials associated with additive/PC electrode reactions, and thermodynamic and kinetic aspects of the consequent chemical reactions. Once the governing factors are unambiguous, the design of electrolyte additives would become more efficient. Another goal is to develop the procedure that could be used for determining the relevant factors of additives and supporting solvents. To illustrate this perspective, we take the known additive VC as an example and analyze extensively the electrochemical and chemical reactions on the basis of quantum chemistry calculations.

Compared with the EC structure, it could be taken for granted that the double bond in VC should be responsible for its efficiency as lithium-ion electrolyte additive. However, besides the aforementioned general uncertainty about its role, a specific question is whether the presence of the double bond improves the electrochemical (E) reaction of solvents or if it just provides more proper passivating products by chemical (C) steps following the electrode reaction, or both. High level density functional theory calculations have been carried out to comprehensively analyze the VC role, starting with the electroreductive decomposition of pure VC in gas phase, and then taking into account the salt effect as well as the solvent effect with the supermolecular models $(VC)Li^+(EC)_n$ ($n = 1-3$).

Computational Details

All the calculations have been performed using the Gaussian 98 program.[9] The equilibrium and transition structures are fully optimized by B3PW91 method[10−13] using 6-311++G(d,p) basis set for the small systems, such as VC and Li^+(VC), whereas 6-31G(d) is used for the larger systems. Single-point energies for the B3PW91/6-31G(d)-optimized geometries have also been calculated at the B3PW91/6-311++g(d,p) level for the systems containing two and more solvent molecules. To confirm the transition states and make zero point energy (ZPE) corrections, frequency analyses are done with the same basis sets as for the geometry optimization. If not noted otherwise, the relative energies refer to those with ZPE correction, and enthalpies and Gibbs free energies are calculated at 298.2 K. Charges are calculated by fitting the molecular electrostatic potential (CHELPG method).[14]

To investigate the role of solvent effects, several strategies are used. In a first stage, specific solvent molecules are explicitly included in the calculations with the molecular clusters $(EC)_nLi^+(VC)$ ($n = 1-3$) in a vacuum. For both $(EC)Li^+(VC)$ and $(EC)_2Li^+(VC)$, the bulk solvent effect is then estimated by a single point calculation using the conductor-like polarizable continuum model (CPCM)[15] and/or the standard dielectric PCM version.[16] In these models, the variation of the free energy when going from vacuum to solution is composed of the work required to build a cavity in the solvent (cavitation energy) together with the electrostatic and nonelectrostatic work (dispersion and repulsion energy),[17] whose sum is referred to as W_0. Additionally, to estimate the contributions from geometry and harmonic vibrations of molecules,

(3) Dominey, L. A. *Lithium Batteries. New Materials, Developments, and Perspectives*; Elsevier: Amsterdam, New York, London, Tokyo, 1994.
(4) Besenhard, J. O.; Fritz, H. P. *J. Electrochem. Soc.* **1974**, *3*, 329.
(5) Aurbach, D.; Levi, M. D.; Levi, E.; Schechter, A. *J. Phys. Chem. B* **1997**, *101*, 2195−2206.
(6) Shu, Z. X.; McMillan, R. S.; Murray, J. J.; Davidson, I. J. *J. Electrochem. Soc.* **1995**, *142*, L161−162.
(7) Jehoulet, C.; Biensan, P.; Bodet, J. M.; Broussely, M.; Tessier-Lescourret, C. In *The Electrochemical Society Proceedings Series*; Holmes, C. F., Landgrebe, A. R., Eds.; Pennington, NJ, 1997; Vol. PV 97-18, p 974.
(8) Wrodnigg, G. H.; Besenhard, J. O.; Winter, M. *J. Electrochem. Soc.* **1999**, *146*, 470−472.
(9) Frisch, M. J.; Trucks, G. W.; Schlegel, H. B.; Scuseria, G. E.; Robb, M. A.; Cheeseman, J. R.; Zakrzewski, V. G.; Montgomery, J. A., Jr.; Stratmann, R. E.; Burant, J. C.; Dapprich, S.; Millam, J. M.; Daniels, A. D.; Kudin, K. N.; Strain, M. C.; Farkas, O.; Tomasi, J.; Barone, V.; Cossi, M.; Cammi, R.; Mennucci, B.; Pomelli, C.; Adamo, C.; Clifford, S.; Ochterski, J.; Petersson, G. A.; Ayala, P. Y.; Cui, Q.; Morokuma, K.; Malick, D. K.; Rabuck, A. D.; Raghavachari, K.; Foresman, J. B.; Cioslowski, J.; Ortiz, J. V.; Stefanov, B. B.; Liu, G.; Liashensko, A.; Piskorz, P.; Komaromi, I.; Gomperts, R.; Martin, R. L.; Fox, D. J.; Keith, T.; Al-Laham, M. A.; Peng, C. Y.; Nanayakkara, A.; Gonzalez, C.; Challacombe, M.; Gill, P. M. W.; Johnson, B. G.; Chen, W.; Wong, M. W.; Andres, J. L.; Head-Gordon, M.; Replogle, E. S.; Pople, J. A. *Gaussian 98*; Gaussian Inc.: Pittsburgh, PA, 1998.
(10) Becke, A. D. *J. Chem. Phys.* **1993**, *98*, 5648−5652.
(11) Perdew, J. P. In *Electronic Structure of Solids*; Ziesche, P., Eschrig, H., Eds.; Akademie Verlag: Berlin, 1991.
(12) Burke, K.; Perdew, J. P.; Wang, Y. *Electronic Density Functional Theory: Recent Progress and New Directions*; Plenum: New York, 1998.
(13) Perdew, J. P.; Burke, K.; Wang, Y. *Phys. Rev. B* **1996**, *54*, 16533−16539.
(14) Breneman, C. M.; Wiberg, K. B. *J. Comput. Chem.* **1990**, *11*, 361.
(15) Barone, V.; Cossi, M. *J. Phys. Chem. A* **1998**, *102*, 1995−2001.
(16) Barone, V.; Cossi, M.; Tomasi, J. *J. Chem. Phys.* **1997**, *107*, 3210−3221.
(17) Cossi, M.; Barone, V.; Cammi, R.; Tomasi, J. *Chem. Phys. Lett.* **1996**, *255*, 327.

Table 1. Structural Parameters (Å for Bond Lengths and deg for Angles) for Vinylene Carbonate[a]

parameter	mw[b]	B3PW91/6-311++G(d,p)	PCM-B3PW91/6-311++G(d,p)[c]	B3LYP/6-311++G(d,p)[19]
C1═O2	1.191	1.185	1.197	1.186
C1−O4	1.364	1.367	1.349	1.372
C6−O4	1.385	1.376	1.384	1.382
C5═C6	1.331	1.328	1.325	1.328
C5−H	1.118	1.076	1.074	1.075
O4−C1−O3	108.8	107.8	108.7	107.7
C6−O4−C1	106.9	107.5	107.4	107.5
O4−C6═C5	108.7	108.6	108.2	108.7
H−C5═C6	133.4	133.6	134.1	133.6

[a] C1,O2 refer to carbonyl group, O3,O4 to ethereal oxygen, C5,C6 to vinylene carbon. [b] Microwave results.[20] [c] Dielectric constant used in the calculations $\epsilon = 110.0$ au, experimental = 127.[30]

geometry optimizations and frequency calculations in the bulk solvent have been done with PCM-B3PW91/6-311++G(d,p) for the two cases such as isolated VC and Li^+(VC) cases. A conventional set of Pauling radii and tetrahedral cavity with 64 initial tesserae has been used for all PCM and CPCM calculations. In this article, we term the above treatment, that is, the continuum model calculation (optimization and/or single point calculation) based on the optimized clusters, as the cluster-continuum model.

To gain insight into the bonding characteristics between Li and solvent molecules, we have also applied the atoms in molecules (AIM) theory of Bader[18] to some species. AIM is based on a topological analysis of the electron density function $\rho(r)$ and of its Laplacian $\nabla^2\rho(r)$ at the bond critical point (bcp). It is well established that the interactions between closed-shell systems (ionic bond, hydrogen bond, van der Waals molecules, etc.) are evidenced by $\nabla^2\rho(r) > 0$, while the inverse $\nabla^2\rho(r) < 0$ corresponds to covalent bonds.

Results and Discussion

A. Reductive Decomposition of VC in Vacuum and Bulk Solvent. In the gas phase as well as in bulk solvent, the calculations show that the ground state of VC (**1**) is planar with C_{2v} symmetry. The structural data from B3PW91/6-311++G(d,p) (summarized in Table 1) very nicely agree (differences less than 0.002 Å and 0.1° for bond lengths and angles, respectively) with a recent B3LYP/6-311++G(d,p) calculation[19] except for two bond lengths of C1O4 and C6O4, for which B3PW91 predicts a value of 0.005 Å shorter than that obtained from B3LYP. The C6O4 distance given by the present DFT results and by microwave spectroscopy data[20] differs by 0.009 Å, and the theoretical and experimental results agree within ±0.005 Å for all the other distances, except for the C−H bond length that is difficult to measure accurately by microwave spectroscopy due to the low hydrogen mass. All of the calculated bond angles agree with microwave experiment and B3LYP calculation within 1°. A small change is observed for the structural parameters using the PCM-B3PW91/6-311+G(d,p) method to study the change from the gas phase to bulk solvent; specifically the bond lengths deviate by less than 0.02 Å and the bond angles by less than 1.0°.

Figure 1 illustrates the selected geometrical parameters of the relevant species, obtained at the B3PW91/6-311++G(d,p) and at PCM-B3PW91/6-6-311++G(d,p) levels on the potential energy surface of the reductive decomposition of VC. The

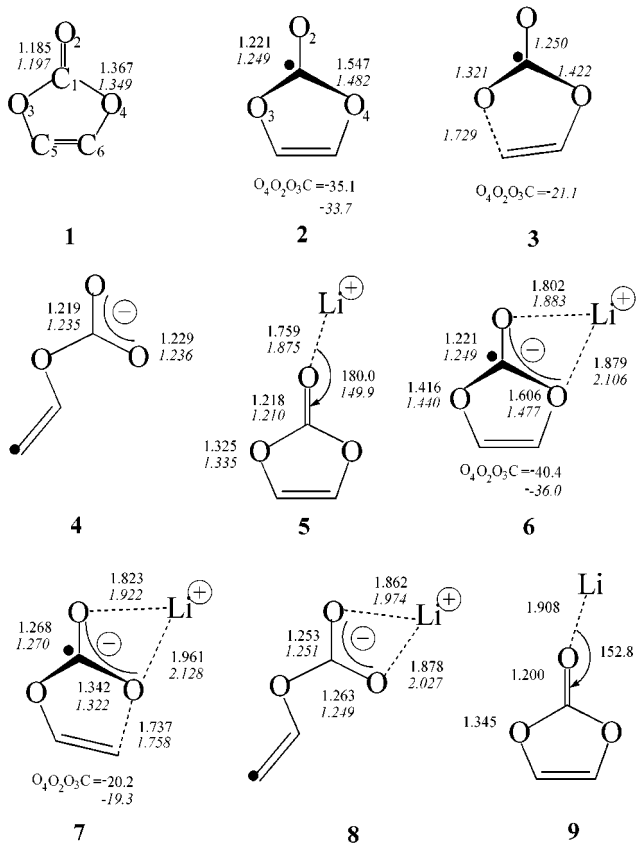

Figure 1. Geometries optimized from B3PW91/6-311++G(d,p) (plain data) and from PCM-B3PW91/6-311++G(d,p) (italic).

relative energies and Gibbs free energies are collected in Table 2 together with their electronic characteristics. The results shown in Figure 1 clearly indicate the changes induced by the solvent on the structure of the reduction intermediate (**2**). For instance, the C1O4 bond is shortened in solvent by 0.07 Å, and the C═O bond is lengthened by about 0.03 Å. In the gas phase, the VC reduction is thermodynamically forbidden as denoted by the positive ΔG (see Figure 2a, +12.8 kcal/mol) between VC and its reductive intermediate as well as the associated negative adiabatic electron affinity ($EA \approx -\Delta E_0$, −13.8 kcal/mol), whereas the reduction intermediate (**2**) is so significantly stabilized by the solvent that the VC reduction is quite plausible in solvent ($\Delta G = -44.7$ kcal/mol, $EA = 45.4$ kcal/mol). The ring-opening reaction of the intermediate **2** proceeds via the transition state **3**, the energy barriers of which are approximately 18.3 and 25.2 kcal/mol in the gas phase and in solvent, respectively. A population analysis on the spin density shows that the unpaired electron mainly locates on the carbonyl carbon in **2** with a coefficient of about 0.8, indicating that VC reduction occurs on the carbonyl carbon. Another evidence of carbonyl carbon reduction is that the CO_3 group in **2** does not keep the planar structure, which is reflected by a clear variation of the dihedral angle (see Figure 1, 4-2-3-1 ∼0.0° in **1** and 33.7° in **2**). It seems likely that the carbonyl C changes from sp^2 in **1** to nearly sp^3 hybridization in **2**. The unpaired electron in **3** is mainly located at the leaving carbon (C6) and at the carbonyl carbon (C1) with coefficients of 0.53 and 0.50 in solvent, respectively. The unpaired electron is totally shifted to the leaving carbon in the radical anion **4**, releasing 58.4 kcal/mol in solvent.

(18) Bader, R. F. W. *Atoms in Molecules, A Quantum Theory*; Clarendon Press: Oxford, 1990.
(19) Autrey, D.; Rosario, A. d.; Laane, J. *J. Mol. Struct.* **2000**, *550−551*, 505−510.
(20) White, W. F.; Boggs, J. E. *J. Chem. Phys.* **1971**, *54*, 4714.

Table 2. Relative Energies, Enthalpies, and Free Energies (in kcal/mol) of the Stationary Points, Charges (*q*/e) of the Carbonyl Carbon Atoms, Spin Densities (*sd*/e) for the Specific Atoms, and Imaginary Frequency (ω/cm^{-1}) of the Ring-Opening Transition States for the VC Reduction Process (Data in Parentheses Refer to Those in Gas Phase)

structures	ΔE^a	$\Delta E_0{}^b$	ΔH^c	ΔG^d	*q*	*sd*[e]	ω
1	0.0	0.0	0.0	0.0	+0.99 (+0.90)		
2	−43.6 (17.0)	−45.4 (13.8)	−44.4 (14.4)	−44.7 (12.8)	+0.02 (−0.03)	0.84 (+0.82)	
3[f]	−21.2 (37.4)	−20.2 (32.1)	−24.1 (32.2)	−20.1 (31.6)	+0.49	0.50/0.53	−1088 (−919, −25)
4	−56.2 (0.63)	−58.4 (−3.6)	−57.4 (−2.6)	−60.0 (−5.3)	+1.1 (+1.0)	/+1.0 (/+0.88)	

[a] ΔE_{tot} (B3PW91/6-311++G(d,p)). [b] ΔE_{tot} (B3PW91/6-311++G(d,p))+ ΔZPE (B3PW91/6-311++G(d,p)). [c] ΔH (298.2 K) (B3PW91/6-311++G(d,p)). [d] ΔG (298.2 K) (B3PW91/6-311++G(d,p). [e] The data before and after slants refer to the carbonyl and leaving ethereal carbon, respectively. [f] The data in gas phase are estimated by B3PW91/6-311++G(d,p)//PCM-B3PW91/6-311++G(d,p), and the vector of $\omega = -919$ cm^{-1} corresponds to the ring opening.

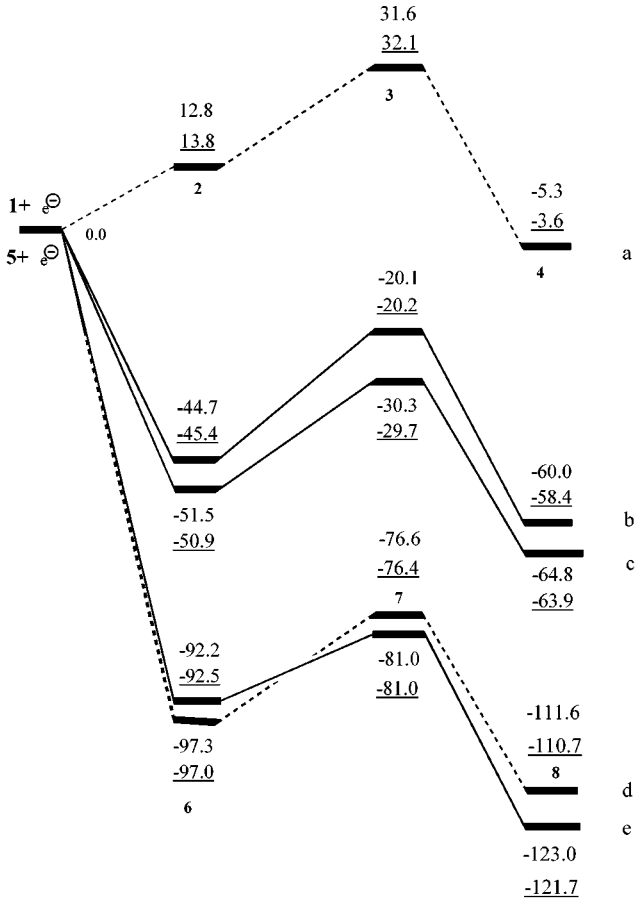

Figure 2. Potential energy (underlined data) and Gibbs free energy (plain data) profile at 298.15 K of the reductive dissociation process. (a) VC in gas phase from B3PW91/6-311++G(d,p). (b) VC in bulk solvent from PCM- B3PW91/6-311++G(d,p). (c) Li^+(VC) in bulk solvent from PCM-B3PW91/6-311++G(d,p). (d) Li^+(VC) in gas phase from B3PW91/6-311++G(d,p). (e) Li^+(EC) in gas phase from B3PW91/6-311++G(d,p).

B. Salt Effect on the Reductive Decomposition of VC in Vacuum and Bulk Solvent. The interaction energies, defined by the energy difference between Li^+(VC) and the total of Li^+ and the VC molecule, are 44.0 and 7.2 kcal/mol (at B3PW91/6-311++G(d,p) and PCM-B3PW91/6-311++G(d,p) levels) in gas and bulk solvent, respectively. A quite strong interaction thereby exists between Li^+ and the VC molecule even in solvent; thus a clear salt effect is expected. Energetic data along the Li^+(VC) reduction primary reaction path are collected in Table 3. Comparing Figure 2d with Figure 2a, the Li^+(VC) (**5**) reductive decomposition proceeds via a qualitatively similar mechanism to that of an isolated VC molecule. However, in sharp contrast, Li^+(VC) (**5**) becomes much more easily reduced to the VC-reduction intermediate **6** in the gas phase with a remarkable *EA* increase (97.0 vs −13.8 kcal/mol). The Li^+-reduction intermediate **9** has also been found, where the unpaired spin density is mainly located at Li instead of at the carbonyl carbon as in **6**. The adiabatic *EA* of Li^+(VC) reduced to **6** is about 4.5 kcal/mol higher than that of Li^+(EC)[21] (as shown in Figure 2d and e, 97.0 vs 92.5 kcal/mol, 4.21 vs 4.01 eV on the physical scale); that is, a more stable reduction intermediate is generated in the case of Li^+(VC), but the barrier of the C−O bond homolytic cleavage via TS **7** is 20.6 kcal/mol, roughly two times higher than that of Li^+(EC). Another difference is that the formation of radical anion **8** releases 11.0 kcal/mol less energy than that of Li^+(EC).

Li^+ separates more from the VC moiety in solvent than in the gas phase, as denoted in Figure 1 by the longer distances between Li^+ and the carbonyl oxygen, as well as from the ethereal oxygen for all the species, which is also reflected by the decrease of $\rho(r)$ and $\nabla^2\rho(r)$ at the bcp between Li^+ and the carbonyl oxygen in solvent (for example, $\rho(r) = 0.041$ au, $\nabla^2\rho(r) = 0.360$ au for **5** in the gas phase vs 0.030 and 0.243 au in solvent). In contrast to the *EA* increase trend of the isolated VC molecule from gas to solvent, a considerable decrease of the adiabatic *EA* of Li^+(VC) is induced by the solvent effect (97.0 vs 50.9 kcal/mol), indicating that in solvent Li^+(VC) is much more stabilized than the intermediate. However, the energy barriers of ring-opening reaction for the intermediate **6** are quite close in the gas phase and solvent (20.6 vs 21.2 kcal/mol); that is, the solvent effect is small on the ring-opening energy barrier, and the latter one is 4.0 kcal/mol lower than that of isolated VC in solvent (21.2 vs 25.2 kcal/mol) arising from the salt (Li^+) effect. The solvent effect leads to a slightly more negative (−1022 vs −1065 cm^{-1}) imaginary frequency in the transition state **7**. Besides the PCM optimizations, the solvent effects on the free energies for the relevant species of Li^+(VC) reductive decomposition are also estimated by C-PCM and D-PCM single point calculations using the geometries optimized in the gas phase. The results are listed in Table 4 together with the relative free energies obtained from the PCM-optimization calculations (ΔG_{sol}). Because C-PCM gives much more consistent errors than D-PCM on nuclear and electronic total polarization charges (with respect to Gauss' law 0.02 ± 0.005, 0.05 ± 0.02), the preceding discussion about bulk solvent effect is mostly based on the C-PCM results, which, despite giving less reliable absolute values of solvent energies, is adequate for the evaluation of relative values between closely related species. Despite the clear difference between some geometrical parameters optimized in the gas phase and in solution, the good agreement between

(21) Wang, Y. X.; Nakamura, S.; Ue, M.; Balbuena, P. B. *J. Am. Chem. Soc.* **2001**, *123*, 11708−11718.

Table 3. Relative Energies, Enthalpies, and Free Energies (in kcal/mol) of the Stationary Points, Charges (*q*/e) of the Lithium Atoms and Carbonyl Groups, Spin Densities (*sd*/e) for the Specific Atoms, and Imaginary Frequency (ω/cm^{-1}) of the Ring-Opening Transition State for the (Li)$^+$VC Reduction Process

					q		*sd*[e]			
structures	ΔE[a]	ΔE_0[b]	ΔH[c]	ΔG[d]	Li	CO_3	C1	Li	C2	ω
5	0.0	0.0	0.0	0.0	+0.98	−0.32				
6	−94.7	−97.0	−96.8	−97.3	+0.83	−0.55	0.76			
7(TS, **6** ↔ **8**)	−72.3	−76.4	−76.3	−76.6	+0.79	−0.93	0.52		0.47	−1022
8	−107.6	−110.7	−110.1	−111.6	+0.83	−0.92			1.00	
9	−91.6	−92.4	−92.7	−93.7	−0.22	−0.18		1.1		
10	−131.3	−135.1	−134.5	−135.8						
11/2	−147.5	−153.1	−148.5	−145.3						
12/2	−134.7	−135.7	−135.4	−131.1						
13/2	−168.5	−168.8	−168.5	−163.2						
14/2	−149.6	−151.4	−150.5	−148.9						

[a] ΔE_{tot} (B3PW91/6-311++G(d,p)). [b] ΔE_{tot} (B3PW91/6-311++G(d,p)) + ΔZPE (B3PW91/6-311++G(d,p)). [c] ΔH (298.2 K) (B3PW91/6-311++G(d,p)). [d] ΔG (298.2 K) (B3PW91/6-311++G(d,p). [e] C1,C2 refer to carbonyl and ethereal carbon, respectively.

Table 4. Solvent Effect Estimated by C-PCM and D-PCM Models for the Electroreductive Decomposition Path of Li$^+$(VC)[a]

structures	ΔG_{vac}	ΔW_0^C	ΔG_{sol}^C	ΔW_0^D	ΔG_{sol}^D	ΔW^D	ΔG_{sol}	ΔG_{sol}[b]	ω[c]
5	0.0	0.0	0.0	0.0	0.0	0.0	0.0	0.0	
6	−97.3	46.7	−50.6	53.3	−44.0	45.8	−51.5	−51.4	
7(TS, **6** ↔ **8**)	−76.6	46.2	−30.4	52.3	−24.3	46.3	−30.3	−30.3	−1065 (−1022)
8	−111.6	47.3	−64.3	49.8	−61.8	51.6	−64.8	−64.5	
9	−93.7	63.5	−30.2	64.0	−29.7				
10	−135.8	−23.5	−159.3	−15.8	−120.0				
11/2	−145.3	51.0	−94.3	50.3	−95.0				
12/2	−131.1	48.3	−82.8	53.3	−77.8				
13/2	−163.2	48.4	−114.8	50.8	−112.4				

[a] Dielectric constant $\epsilon = 111.0$; ΔG_{vac} and ΔG_{sol} refer to the Gibbs free energies in the gas phase and in the solution at 298.15 K, respectively; ΔW_0^D and ΔW_0^C refer to the free energy contributions from D-PCM and C-PCM-B3PW91/6-311++G(d,p)// B3PW91/6-311++G(d,p); ΔW^D includes also the contributions provided by geometry variation and by vibrational frequency variation. [b] D-PCM-B3PW91/6-311++G(d,p), $\epsilon = 89.78$ of pure EC at room temperature. [c] The imaginary frequency in parentheses refers to that in the gas phase.

C-PCM relative free energies (ΔG_{sol}^C, the fourth column in Table 4) with those of ΔG_{sol} (the eighth column) shows that the majority of the solvent stabilizing effects are obtained using gas-phase structures. Terminations of the radical anion **8** would take place, either by dimerization or by reactions with other involved species such as intermediates and reactants (shown in Figure 3). A carbon anion of intermediate **10**, which was not located for Li$^+$(EC), is generated by further reduction of **8**. Intermediate **10** could further decompose into $(LiCO_3)^-$ and acetylene gas ($\Delta G = -24.1$ kcal/mol at B3PW91/6-311++G(d,p)), and it may also undergo several further reactions with quite negative ΔG, such as the barrierless ion-pairing reactions with Li$^+$(VC) to generate lithium carbonate (**14**) and a lithium carbide compound (**12**), and nucleophilic addition to Li$^+$(VC) giving rise to lithium divinylene dicarbonate (**13**). Other termination reactions of **8** are generally more favorable than the corresponding reactions in the case of Li$^+$(EC);[21] for example, the dimerization reaction to generate lithium vinylene dicarbonate **11** has 10.4 kcal/mol lower ΔG (−67.2 vs −56.8 kcal/mol), and the formation reaction of C−Li carbide compound **12** has a much lower ΔG (−56.9 vs −39.6 kcal/mol). More surprisingly, the ΔG of the dimerization reaction ending in another lithium dicarbonate **13** is even 50% lower (ΔG, −103.2 vs −67.4 kcal/mol). The extra stability of the dimers may be due to electron delocalization in the conjugated group, −CH═CH−CH═CH. The VC reduction therefore has a different product distribution than EC;[21] specifically the C−Li carbide (**12**) and the lithium alkyl dicarbonate with the long chain (**13**) are more likely to be found. Similar to the effect described for the ring-opening energy barrier, that of the bulk solvents from C-PCM on the ΔG of the termination reactions of **8** (see Figure 3) is not significant.

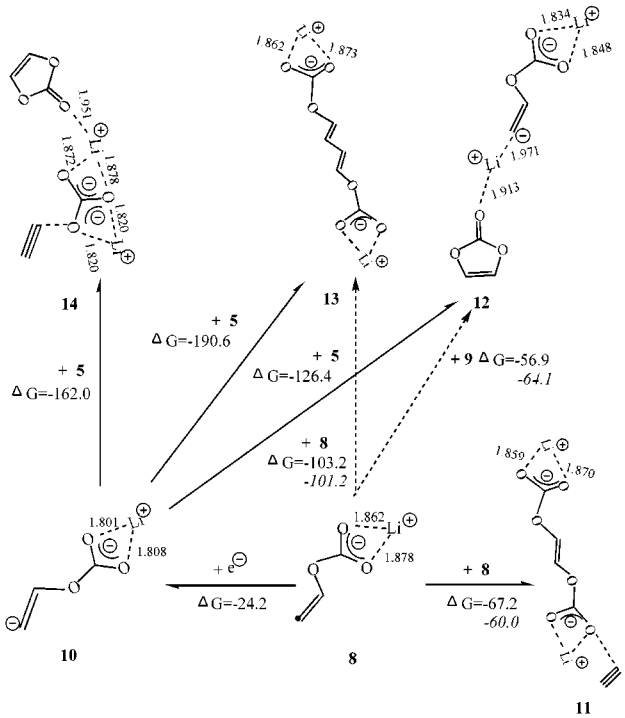

Figure 3. Termination reactions of the radical anion from the decomposition of Li$^+$(VC), from B3PW91/6-311++G(d,p). Plain and italic data refer to the variations of Gibbs free energy in the gas phase and in solvent, respectively.

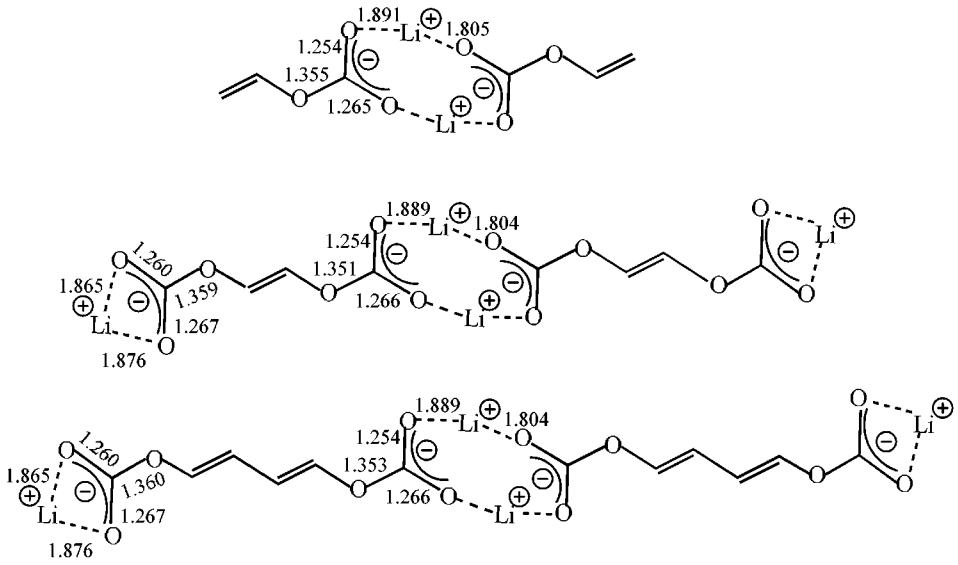

Figure 4. Dimers of lithium vinylene carbonate (LVC), lithium vinylene dicarbonate (**11**), and lithium divinylene dicarbonate (**13**) with B3PW91/6-31G*.

Very recently Ross et al.[22] examined experimentally the electroreductions of VC, EC, PC, dimethyl carbonate (DMC), and diethyl catbonate (DEC) on the gold surface (1 vol % target solvent species, supporting electrolyte, THF/0.1 M $LiClO_4$) using cyclic voltammetry (CV) and FTIR techniques. The measured reduction potential for VC is 1.40 V (vs Li^+/Li), or −2.96 eV on the physical scale. We calculated the reduction potentials for the following electron-transfer reactions:

$$(VC)\cdots Li^+ \ (\mathbf{5}) + e^- \rightarrow [(VC)^{\bullet -}]\cdot\cdot Li^+ \ (\mathbf{6}) \qquad \text{(I)}$$

$$(VC)\cdots Li^+ \ (\mathbf{5}) + e^- \rightarrow H\overset{\bullet}{C}H(CO_3)^- Li^+ \ (\mathbf{8}) \qquad \text{(II)}$$

(ΔG_{vac}: −97.3 and −111.6 kcal/mol in Table 3, respectively, and −4.2 to −4.8 eV on the physical scale) which in the gas phase are too negative as compared with the experimental values. The reduction potentials, especially for reaction II, in bulk solutions (ΔG_{sol}^{C}: −50.6 and 64.3 kcal/mol, about −2.19 and −2.79 eV on the physical scale) are similar to the experimental reduction potential of VC on the gold electrode in the presence of the Li salt, but it needs to be confirmed by more realistic models than Li^+(VC)-PCM.

The new IR peaks showed a ring opening of VC after solvent reduction,[22] and a broad shoulder at 980 cm^{-1} was assigned to the out-of-plane C−H bending mode of a methylene ($=CH_2$) group. They claimed therefore that lithium vinylene carbonate (LVC) is a major component in the organic layer of the SEI. In line with the present results, the suggested reduction mechanism also includes initially the formation of the radical anion (**8**), but then the radical anion undergoes a hydrogen abstraction to produce lithium vinylene carbonate (LVC). As demonstrated by Matsuta et al.[23] for the dimerization of lithium alkyl carbonates ($ROCO_2Li$), lithium dicarbonates, **11** and **13**, could also aggregate to eight-membered-ring species (dimer, trimer, etc.) via intermolecular interactions between Li^+ and O (see Figure 4). The dimerization energies are as high as 42.3, 42.7, and 42.8 kcal/mol (at B3PW91/6-31G* after ZPE and basis set superposition error correction) for LVC, **11** and **13**, respectively, which suggests that lithium alkyl dicarbonates probably exist in the SEI layer in the form of polymer-like species with repeated eight-membered-ring units. Frequency analyses are conducted to identify reduction products of VC, using HF/6-31G*//B3PW91/6-31G* with a scaling factor of 0.8929 to compensate for the well-known overestimation given by the HF-SCF method. The harmonic vibrational frequencies for LVC, **11**, **13**, and their dimers are summarized in Table 5. The remarkable frequency changes occur in the eight-membered-ring, for example, blue shifts of 30−40 cm^{-1} of CO_2 asymmetric stretching, and blue shifts (about 60 cm^{-1} for LVC, 30 cm^{-1} for **11**, and 20 cm^{-1} for **13**) of LiO stretching, which are in line with the corresponding bond shortening induced by the dimerization. As expected, Table 5 also shows that the leading peaks between **11** and **13** agree very well, and they are also close to those of LVC. Especially the C−O stretchings in the dimer of **13** (950 cm^{-1}) and the dimer of **11** (938 cm^{-1}) locate around the peak of 950 cm^{-1} (experimental 980 cm^{-1}) assigned to the CH_2 out-of-plane bending in LVC. Therefore, LVC could be produced in the scheme suggested by Ross et al.;[22] however, the existence of **11** and **13** could also be deduced from the experimental spectra.

Whether VC could form polymeric compounds is another related problem. Two possible polymerization mechanisms are evaluated (Figure 5). One is initiated by the radical anion (**8**), the other by the carbon anion (**10**), which are absent in the case of Li^+(EC) due to shortage of the C=C double bond. Reaction Ia has a considerable negative ΔG (−39.0 kcal/mol at B3PW91/6-31G*), while that of Ib becomes positive ($\Delta G > 0$) due to entropy loss, indicating that the oligomers with two and three vinylene units could be generated by reaction Ia and that the generation of the oligomers with more vinylene units is forbidden. IIa has a similar ΔG (−175.0 kcal/mol at B3PW91/6-31G*) to the other two reactions in Figure 3 where both anion **10** and Li^+(VC) are involved. Similar to the pattern of the

(22) Zhang, X. R.; Kostecki, R.; Richardson, T. J.; Pugh, J. K.; Ross, P. N. *J. Electrochem. Soc.* **2001**, *148*, A1341−1345.
(23) Matsuta, S.; Asada, T.; Kitaura, K. *J. Electrochem. Soc.* **2000**, *147*, 1695−1702.

Table 5. Characteristics of the Calculated Frequencies (cm^{-1}) for Several Kinds of Lithium Alkyl Carbonates with HF/6-31G*//B3PW91/6-31G*

assignments[a]	LVC	D1	11	D2	13	D3
CH sym/asym stretching	2983	2986,[b] 2986	2983,[b] 2976	2984,[b] 2984[b]	2959,[b] 2959	2963,[b] 2963, 2958,[b] 2957
	2959	2963,[b] 2963		2976,[b] 2976		
	2906[b]	2907,[b] 2907[b]			2904, 2898[b]	2906,[b] 2906, 2899,[b] 2899[b]
C═C stretching	1640	1641,[b] 1641	1674[b]	1674,[b] 1674[b]	1677[b]	1677,[b] 1677[b]
					1606	1606,[b] 1606
CO_2(Li) asym stretching	**1501**	**1538, 1531**[b]	**1498**[b]	**1534, 1526**[b]	**1500**[b]	**1535, 1528**[b]
			1495	1502,1502[b]	1498	1503, 1503
CH_2 scissoring	1412	1411,[b] 1411				
C1O stretching			1360[b]	1367,[b] 1357		
C1O stretching, CH i.p. rock	1325	1343,[b] 1317	1322	1327,[b] 1321	1358[b]	1362,[b] 1358
			1288	1292,[b] 1278	1336,[b] 1311, 1291	1343,[b] 1333, 1317,[b] 1304, 1293,[b] 1288
CH i.p. rock	1293	1296,[b] 1294	1268[b]	1270,[b] 1270[b]	1271,[b] 1246	1273,[b] 1272, 1246,[b] 1246
C2O stretching	1151	1151,[b] 1148	1140,[b] 1135	1144,[b] 1143,[b] 1142,[b] 1136		
C−C stretching					1161[b]	1163,[b] 1163[b]
C2O stretching	1036	1056, 1053[b]			1148,[b] 1096	1150,[b] 1149,[b] 1120,[b] 1098
C−H o.p. bending	1038	1033, 1033[b]	1001	1001, 1000[b]	1027, 985[b]	1026, 1026,[b] 984,[b] 984[b]
C1−O stretching			989[b]	1003, 1000[b]	954	970, 966[b]
CH_2 o.p. bending	942	950, 950[b]				
C1−O stretching	895[b]	897, 894[b]	931	938,[b] 936[b]	948[b]	951, 950[b]
CH o.p. bending			900[b]	899,[b] 899[b]	917,[b] 882[b]	917,[b] 917,[b] 881,[b] 881[b]
CO_3 bending	841	839, 837[b]	839, 839[b]	838, 838,[b] 837, 834[b]	840, 840[b]	840, 840,[b] 836, 836[b]
CO_2 bending			756,[b] 728	751,[b] 747, 741,[b] 732[b]	754, 727[b]	755,[b] 751, 732,[b] 724
CH,CH_2 o.p. wagging	746[b]	746,[b] 745[b]				
CO_2(Li) bending	732	744,[b] 732[b]				
CO_2(Li) bending, LiO stretching					642,[b] **605**	660, 654[b] **625, 623**[b] 606
LiO stretching	**591**	**650, 616**[b]	**620**	**655, 648**[b]	584, 564[b]	574,[b] 570, 553[b]
CO_2 bending			619[b]	624, 611[b]		
LiO stretching	551	555,[b] 528[b]	578,[b] 537	599, 566,[b] 543,[b] 541		478,[b] 460,[b] 451, 446[b]
CO_2Li rocking	420	447,[b] 419[b]	453, 413[b]	447,[b] 443,[b] 379	464,[b] 455, 411	478,[b] 460,[b] 451, 446[b]
CH═CH o.p. bending			367[b]	367,[b] 367[b]	394[b]	395,[b] 395[b]
CO_2Li rocking	390			367[b]	351[b]	386, 379[b]
LiLi stretching		312[b]		346[b]		321[b]

[a] C1 and C2 refer to the carbonate and alkyl group, respectively; i.p. and o.p. are abbreviations to in-plane and out-of-plane. [b] The relative intensities are less than 0.01.

reaction I, the ΔG of reaction IIb is considerably increased to −5.1 kcal/mol, although it is still thermodynamically possible. Thus, the reactions via anion attacking carbonyl carbon could only give rise to oligomers with low order carbonate-vinylene units.

C. Interplay between EC and VC in the Cluster (EC)-Li^+(VC). It is well accepted that the current polarized continuum models (PCM) are adequate to describe reactions in solution unless some solvent molecules are involved in the reaction mechanism. The fact that a quite strong interaction also exists between Li^+ and the EC molecule causes us to reinvestigate the reduction of VC in the presence of one explicit EC molecule, from which some insights about the effect of VC on the reduction of EC could also be obtained. The reduction path of the cluster (EC)Li^+(VC) and the subsequent termination reactions are shown in Figure 6a,b,c, and the corresponding energetic data are listed in Table 6. Besides the intermediate of Li^+ being reduced, that is, (EC)Li(VC) (**19**, not shown in Figure 6a), the ion-pair reduction intermediates such as **16**, **17**, and **18** (not shown in Figure 6a) have been located, which correspond to the reductions of EC, VC, and both molecules, respectively. Intermediate **17** has the lowest energy (*EA*, 77.4 kcal/mol, as in Table 6), followed by **16** (*EA*, 74.3) and **18** (*EA*, 73.9), and **19** (*EA*, 64.7) the highest. Qualitatively consistent with the previous CPCM calculations for Li^+(VC), the *EA* related to the VC-reduction intermediate **17** is considerably decreased (77.4 vs 97.0 kcal/mol) arising from the solvent effect by explicitly including one EC molecule, as is the *EA* related to the EC-reduction intermediate **16** (74.3 vs 92.5 kcal/mol). Bulk solvent effects, incorporated by C-PCM and D-PCM using the gas-phase

Table 6. Relative Energies, Enthalpies, and Free Energies (in kcal/mol) of the Stationary Points, Charges (*q*/e) of the Lithium Atoms and EC or VC Moiety, Spin Densities (*sd*/e) for the Specific Atoms, and Imaginary Frequency (ω/cm^{-1}) of the Ring-Opening Transition State for the (EC)Li$^+$(VC) Reduction Process[a]

						q		*sd*[g]			
structures	ΔE[b]	$\Delta E(0)$[c]	ΔE_0[d]	ΔH(T)[e]	ΔG(T)[f]	Li	EC(VC)	C1	Li	C2	ω
15	0.0	0.0	0.0	0.0	0.0	+0.95	+0.03 (+0.02)				
16	−69.6	−71.5	−74.3	−74.6	−72.7	+0.77	−0.82 (+0.05)	0.67	0.08	0.15	
17	−71.7	−73.9	−77.4	−77.4	−75.8	+0.77	+0.05 (−0.82)	(0.65)	0.06	(0.13)	
18	−68.3	−70.0	−73.9	−74.5	−69.0	+0.79	−0.38 (−0.41)	0.24 (0.33)		0.10 (0.11)	
19	−59.4	−61.5	−64.7	−64.3	−64.6	−0.22	+0.18 (+0.05)		0.79		
20(TS, **16** ↔ **21**)	−55.3	−59.1	−63.2	−63.5	−61.6	+0.71	−0.77 (+0.06)	0.43	0.10	0.41	−918
21	−94.1	−98.7	−104.2	−103.4	−104.0	+0.72	−0.80			1.1	
22(TS, **17** ↔ **24**)	−48.7	−52.7	−57.0	−57.0	−55.7	+0.73	(−0.79)	(0.38)		(0.46)	−1009
23(TS, **17** ↔ **21**)	−54.2	−58.7	−63.9	−63.7	−63.3	+0.67	−0.27 (−0.41)	(0.41)	0.15	0.30	−759
24	−83.1	−86.2	−91.8	−91.3	−91.1						
25	−134.7	−140.3	−154.2	−153.6	−151.8						
26/2	−126.8	−129.0	−133.7	−132.9	−128.0						
27/2	−140.0	−140.6	−144.4	−144.5	−136.7						
28/2	−106.7	−108.1	−110.9	−110.7	−103.1						
29/2	−125.6	−126.0	−128.5	−128.8	−118.9						
30/2	−126.8	−128.8	−132.5	−131.9	−125.0						
31/2	−127.5	−129.6	−134.1	−133.2	−127.5						
32	−109.5	−113.3	−127.0	−127.2	−122.1						
33/2	−145.3	−145.6	−149.2	−149.3	−140.6						
34/2	−120.6	−122.6	−128.2	−127.5	−121.3						
35/2	−141.3	−141.8	−145.6	−145.4	−138.1						
36/2	−111.6	−111.9	−114.7	−114.6	−106.4						

[a] The charges (*q*/e) and spin densities (*sd*) in parentheses refer to the VC moiety or to the corresponding atoms of the VC moiety. [b] ΔE (B3PW91/6-31G(d)). [c] $\Delta E(0)$: ΔE (B3PW91/6-31G(d)) + ΔZPE (B3PW91/6-31G(d)). [d] ΔE_0: ΔE (B3PW91/6-311++G(d,p)//B3PW91/6-31G(d)) + ΔZPE (B3PW91/6-31G(d)). [e] ΔH, ΔE (B3PW91/6-311++G(d,p)//B3PW91/6-31G(d)) + $\Delta\Delta H$ (B3PW91/6-31G(d)). [f] ΔG, ΔE (B3PW91/6-311++G(d,p)//B3PW91/6-31G(d)) + $\Delta\Delta G$ (B3PW91/6-31G(d). [g] C1,C2 refer to carbonyl and ethereal carbon, respectively.

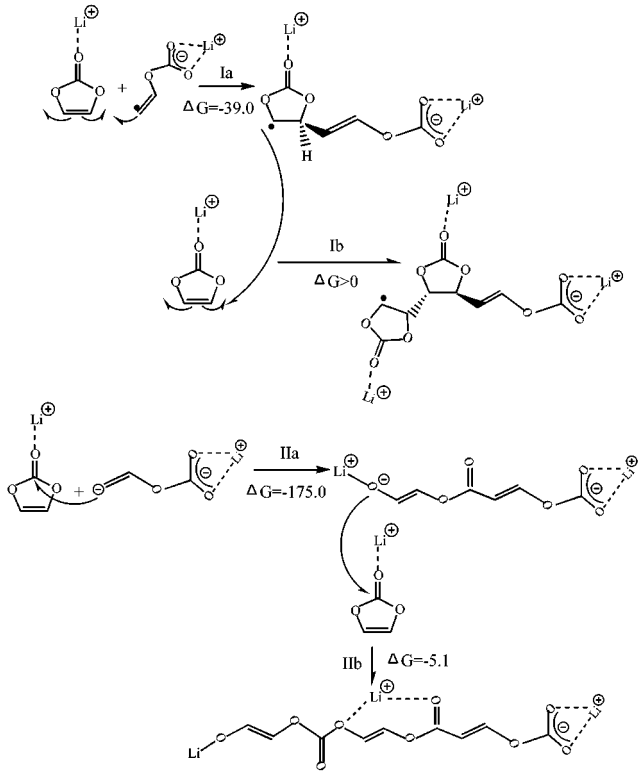

Figure 5. Reactions of radical anion (**8**) and carbon anion (**10**) with Li$^+$-(VC), and their Gibbs free energy changes with B3PW91/6-31G*.

optimized geometries (as shown in Table 7), further remarkably decrease their *EA*s, and the *EA* difference between **17** and **16** is enhanced to 6.2 kcal/mol ($EA \approx -\Delta E_{sol}^{C}$, 52.1 vs 45.9 kcal/mol from C-PCM), which shows that the solvent effect facilitates the formation of the VC-reduction intermediate. Table 7 also shows that the cluster-CPCM predicted reduction potentials (ΔG_{sol}^{C}) of VC- and EC-reduction corresponding to the electrode reactions III−VI,

$$(EC)\cdots Li^+\cdots(VC)\,(\mathbf{15}) + e^- \rightarrow (EC)\cdots Li^+\cdots[(VC)^{\bullet -}]\,(\mathbf{17}) \quad \text{(III)}$$

$$(EC)\cdots Li^+\cdots(VC)\,(\mathbf{15}) + e^- \rightarrow (EC)\cdots Li^+\cdots(CO_3)^-CH_C^{\bullet}H\,(\mathbf{24}) \quad \text{(IV)}$$

$$(EC)\cdots Li^+\cdots(VC)\,(\mathbf{15}) + e^- \rightarrow [(EC)^{\bullet -}]\cdots Li^+\cdots(VC)\,(\mathbf{16}) \quad \text{(V)}$$

$$(EC)\cdots Li^+\cdots(VC)\,(\mathbf{15}) + e^- \rightarrow H_2C^{\bullet}CH_2(CO_3)^-\cdots Li^+\cdots(VC)\,(\mathbf{21}) \quad \text{(VI)}$$

are − 48.0, −61.6, −43.6, and − 73.3 kcal/mol, respectively, (−2.08, −2.67, −1.89, and −3.19 eV on the physical scale), which are 2−3 kcal/mol less negative than the corresponding ones obtained from Li$^+$(VC)-CPCM (−50.6 and −64.3 kcal/mol) and Li$^+$(EC)-CPCM (−45.8 and −75.8 kcal/mol,[21] see also Table 9). Coupled with the considerable *EA* decrease (∼20.0 kcal/mol) by adding one more explicit solvent molecule, we could conclude that a cluster-continuum model is necessary including both specific and bulk solvent effects. It is worth noting that theoretical reduction potentials based on the formation of ion-pair intermediates (**16** and **17** from reactions III and V, respectively) qualitatively reproduce the experimental trend that VC has a more negative reduction potential of physical scale on gold electrode surface,[22] whereas those based on the anion radicals (**21** and **24** from reactions IV and VI) provide

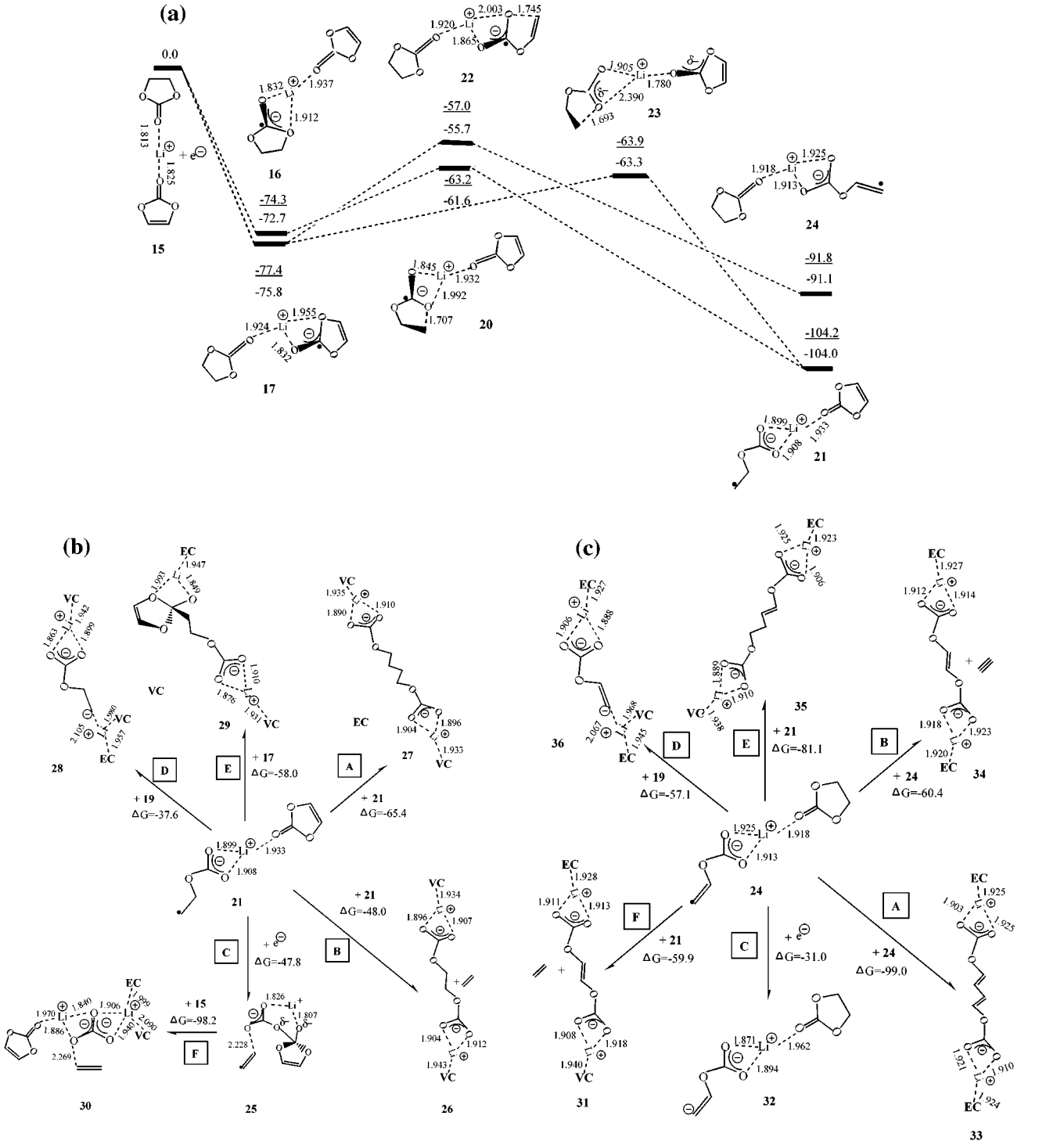

Figure 6. (a) Potential energy (underlined data) and Gibbs free energy profile at 298.15 K for the reductive decomposition process of (EC)Li$^+$(VC) calculated with B3PW91/6-311++G(d,p)// B3PW91/6-31G(d). (b) Termination paths for the radical anion from the EC reductive dissociation in (EC)Li$^+$(VC) calculated with B3PW91/6-311++G(d,p)//B3PW91/6-31G(d) method. (c) Termination paths for the radical anion from the VC reductive dissociation in (EC)Li$^+$(VC) calculated with the B3PW91/6-311++G(d,p)//B3PW91/6-31G(d) method.

an opposite result. The latter reduction potentials of VC and EC (−2.67 and −3.19 eV) are numerically close to the CV measured reduction potentials on the gold electrode of about −2.96 eV of VC, and −2.92 eV of EC.[22] Either the reduction potential of EC obtained via CV,[24] or the voltage value of potential-capacity plot corresponding to the SEI film initial formation, on the graphite surface, lies in the range of −2.36 to −2.56 eV,[25−27] and deviates significantly from that on the

(24) Jeong, S.-K.; Inaba, M.; Abe, T.; Ogumi, Z. *J. Electrochem. Soc.* **2001**, *148*, A989−A993.

(25) Naji, A.; Ghanbaja, J.; Humbert, B.; Willmann, P.; Billaud, D. *J. Power Sources* **1996**, *63*, 33−39.

(26) Novak, P.; Joho, F.; Imhof, R.; Panitz, J.-C.; Haas, O. *J. Power Sources* **1999**, *82*, 212−216.

Table 7. Solvent Effect Calculated from C-PCM and D-PCM Models (Dielectric Constant $\epsilon = 89.78$, Pauling Radii), ΔE_{vac} (ΔG_{vac}) and ΔE_{sol} (ΔG_{sol}) Refer to the Energies (Gibbs Free Energies) in the Gas Phase and in Solution, Respectively; ΔW_0^D and ΔW_0^C (ΔE_0^C) Refer to the Contributions from D-PCM and C-PCM-B3PW91/6-311++G(d,p)// B3PW91/6-31G(d)[a]

structures	ΔE_{vac}	ΔG_{vac}	ΔE_0^C	ΔW_0^D	ΔW_0^C	ΔE_{sol}^C	ΔG_{sol}^D	ΔG_{sol}^C
15	0.0	0.0	0.0	0.0	0.0	0.0	0.0	0.0
16	−74.3	−72.7	28.4	27.0	29.1	−45.9	−45.7	−43.6
17	−77.4	−75.8	25.3	33.7	27.8	−52.1	−42.1	−48.0
18	−73.9	−69.0	29.7		32.5	−44.2		−36.5
19	−64.7	−64.6	37.1	41.4	37.9	−23.3	−23.2	−26.7
20(TS, **16** ↔ **21**)	−63.2	−61.6	27.3	26.0	28.4	−35.9	−35.6	−33.2
21	−104.2	−104.0	29.4	33.5	30.7	−74.8	−70.5	−73.3
22(TS, **17** ↔ **24**)	−57.0	−55.7	27.5	33.2	28.2	−29.5	−22.5	−27.5
23(TS, **17** ↔ **21**)	−63.9	−63.3	29.6	35.3	30.5	−34.3	−28.0	−32.8
24	−91.8	−91.1	28.2	28.6	29.5	−63.6	−62.5	−61.6

[a] With respect to the structure **15**, $W_0^D = -46.4$ kcal/mol, $W_0^C = -47.9$ kcal/mol, $E_0^C = -52.9$ kcal/mol.

Table 8. As in Table 6 Except for Different Structures from $(EC)_2Li^+(VC)$ and $(EC)_3Li^+(VC)$

						q		*sd*		
structures	ΔE	$\Delta E(0)$	ΔE_0	$\Delta H(T)$	$\Delta G(T)$	Li	EC(VC)	C1	C2	ω
					$(EC)_2Li^+(VC)$					
37	0.0	0.0	0.0	0.0	0.0	+0.88				
38	−63.5	−65.2	−70.1	−70.3	−66.0	+0.64	(−0.61)	(0.67)		
39	−58.0	−59.6	−64.0	−64.4	−59.1	+0.66	−0.67	0.68		
40(TS, **38** ↔ **43**)	−40.4	−44.2	−50.0	−50.3	−45.3	+0.66	(−0.67)	(0.40)	(0.47)	−1022
41(TS, **39** ↔ **44**)	−45.5	−49.1	−55.2	−55.7	−50.6	+0.66	−0.67	0.44	0.43	−900
42(TS, **38** ↔ **44**)	−42.8	−46.9	−52.9	−53.2	−48.4	+0.67	−0.34 (−0.36)	(0.41)	0.38	−764
43	−71.8	−74.7	−81.4	−81.2	−78.2					
44	−81.8	−85.9	−92.2	−91.8	−88.6					
					$(EC)_3Li^+(VC)$					
45	0.0	0.0	0.0	0.0	0.0	+0.98				
46	−58.2	−59.9	−64.1	−63.9	−61.5	+0.66	(−0.56)	(0.64)		
47	−52.5	−54.1	−58.8	−58.3	−54.8	+0.69	−0.67	0.70		
48	−55.5	−56.9	−60.3	−60.1	−55.0	+0.63	−0.32 (−0.31)	0.29 (0.24)		
49(TS, **46** ↔ **52**)	−34.3	−38.0	−43.0	−42.3	−39.4	+0.64	(−0.62)	(0.47)	(0.39)	−1040
50(TS, **46** ↔ **53**)	−36.2	−40.0	−45.7	−45.0	−42.4	+0.67	−0.33 (−0.36)	(0.43)	0.35	−784
51(TS, **47** ↔ **53**)	−39.4	−43.0	−48.7	−48.2	−44.2	+0.74	−0.70	0.43	0.44	−928
52	−67.5	−70.4	−77.0	−76.2	−73.2					
53	−75.6	−79.4	−85.4	−83.9	−83.5					

Table 9. Comparisons between Bond Lengths (*R*/Å at B3PW91/6-31G(d)), Binding Energies per Solvent Molecule (*BE*/kcal/mol at B3PW91/6-31G(d)), Adiabatical Electron Affinity (*EA*/kcal/mol), Ring-Opening Barriers (E_a/kcal/mol), Releasing Energies (*RE*) of Radical Anion Formation for $Li^+(EC)_n$ ($n = 1-4$), and $(EC)_nLi^+(VC)$ ($n = 0-3$)

structures	*R*	*BE*	*EA*[b]	E_a[c]	*RE*[d]
$Li^+(EC)$	1.764	50.3	92.5/45.9	11.5/9.6	121.7/75.8
$Li^+(EC)_2$	1.814	44.7	72.4/45.2	11.0/10.5	102.3/73.3
$Li^+(EC)_3$	1.893	37.8	64.6	11.1	93.9
$Li^+(EC)_4$	1.965	32.2	59.0	10.2	86.9
$Li^+(VC)$	1.773	46.4	97.0/50.9	20.6/21.2	110.7/64.3
$(EC)Li^+(VC)$	1.813, 1.825	43.1	77.4 (74.3)/52.1 (45.9)	11.1/10.0	104.2/74.8
				20.4/22.6	91.8/63.6
				13.5/17.8	
$(EC)_2Li^+(VC)$	1.888, 1.903	37.0	70.1 (64.0)	8.8	92.2
				20.1	81.4
				17.2	
$(EC)_3Li^+(VC)$	1.956[a], 1.981	31.7	64.1 (58.8)	10.1	85.4
				21.1	77.0
				18.4	

[a] Average of the three $Li^+\cdots O$ interactions. [b] The data outside and in parentheses for $(EC)_nLi^+(VC)$ correspond to the reductions of VC and EC, respectively. The data before and after slants refer to without and with CPCM corrections, respectively. [c] The first two data for $(EC)_nLi^+(VC)$ correspond to the ring-opening of EC and VC in their respective reduction-intermediate; the third one corresponds to the ring-opening of EC in the VC-reduction intermediate. [d] The two data for $(EC)_nLi^+(VC)$ correspond to the ring-opening of EC and VC; the results of $Li^+(EC)_n$ from ref 21.

gold surface. The theoretical incorporation of the electrode effect on the reduction potentials is underway.

Comparing Figure 6a with Figure 2d and e, we observe that the solvent effect from one explicit EC molecule on the ring-opening barrier is negligible; for example, that of the intermediate **17** (TS, **22**) is nearly the same as that of the simple model $Li^+(VC)$, (20.4 vs 20.6 kcal/mol). The same pattern is observed for the EC reduction intermediate, **16**; its energy barrier (TS, **20**) remains also rather close to $Li^+(EC)$[21] (11.1 vs 11.5 kcal/mol). Although **16** has 3.1 kcal/mol higher energy than **17** in

(27) Yamaguchi, S.; Asahina, H.; Hirasawa, K. A.; Sato, T.; Mori, S. *Mol. Cryst. Liq. Cryst.* **1998**, *322*, 239−244.

the gas phase, the ring opening of the former results in a more stable radical anion (**21**) than the latter (**24**) by 12.4 kcal/mol. Of particular interest on the potential energy surface of Figure 6a is the homolytic ring opening of EC on the intermediate **17**, bringing about the more stable radical anion **21**, via an intramolecular electron-transfer transition state **23**, where the unpaired spin density is located at the carbonyl carbon of VC with a coefficient of 0.41, and at the leaving ethereal carbon of EC with 0.30, and at the lithium atom with 0.15 (Table 6). The characteristics of **23** as a transition state connecting **17** and **21** have been confirmed by the vibrational modes of its eigenvectors as well as by IRC calculations. The energy barrier of **17** via TS **23** is only 13.5 kcal/mol, which is 6.9 kcal/mol lower than the opening of VC via TS **22**, and it is only 2.4 kcal/mol higher than the homolytic ring opening of **16** via TS **20**. The bulk solvent effect predicted by a C-PCM single point calculation (see Table 7) slightly decreases the ring-opening energy barrier of **16** (10.0 vs 11.1 kcal/mol), whereas it largely affects the two ring-opening channels of **17**; specifically the ring-opening barriers of VC and EC are enhanced to 22.6 and 17.8 kcal/mol, respectively. It is interesting, however, that the relative trend of the barriers for the ring opening of **16** and **17** still remains in the bulk solvent. Taking into account thermodynamic as well as kinetic aspects of the ring opening for the supermolecule $(EC)Li^+(VC)$, we could conclude that the optimal reductive decomposition path of $(EC)Li^+(VC)$ in both the gas phase and solution is initially reduced to the most stable ion-pair intermediate **17** by VC reduction. However, to avoid overcoming a high energy barrier, a homolytic ring opening will then take place in the EC moiety instead of on the reduced VC via an intramolecular electron-transfer TS **23**, generating the more stable radical anion **21**. For the decomposition process, VC is not consumed; it just catalyzes the homolytic ring opening of EC via the formation of a stable ion-pair intermediate.

Regarding the termination reactions of the radical anion **21** shown in Figure 6b, its further reduction by the second electron from the polarized anode yields **25** (path C in Figure 6b), where the carbonyl carbon in VC tends to combine with the EC ethereal oxygen due to easier reduction of VC compared to EC, that is, recombination may take place in **25** after accepting another electron. The ion-pairing reaction (path F) of **25** with $(EC)Li^+(VC)$ to generate lithium carbonate (**30**) has a quite comparable ΔG (−97.0 vs −98.2 kcal/mol) to that from $(LiCO_3)^-$ in the case of $Li^+(EC)_2$.[21] Regarding other termination reactions of the radical anion **21**, the differences of ΔG with the corresponding reactions of $Li^+(EC)_2$ are only about 1.0 kcal/mol, for example, 0.3 kcal/mol more for the Li carbide (**28**) generation, 0.6 and 1.4 kcal/mol less for lithium ethylene dicarbonate (**26**) and lithium butylene dicarbonate (**27**), respectively, and nearly identical for the R−O−Li compound (**29**). This implies that the major effect of VC lies in the initial step of the solvent reduction.

The effect of the EC molecule on the termination reactions of radical anion **24** is also investigated, as shown in Figure 6c. The ΔG of the further reduction to **32** becomes 6.8 kcal/mol more negative as compared with that of $Li^+(VC)$. The two paths resulting in lithium alkyl dicarbonates (**33** and **34**) exhibit 4.2 and 6.8 kcal/mol less negative ΔG, respectively, which qualitatively agrees with the CPCM predictions for $Li^+(VC)$. As to the C−Li carbide generation path, there is only a slight change (−57.1 vs −56.9 kcal/mol). The ΔG of path E to form lithium alkyl dicarbonate (**35**) through the cross dimerization of **24** with the radical anion **21** is considerably higher than that of path A (−81.1 vs −99.0 kcal/mol), which reveals the crucial role of the unsaturated group in stabilizing these dicarbonates through electron delocalization. Another path (F) through the cross dimerization of **24** with **21** to form **31** has a ΔG rather close to path B (−59.9 vs −60.4 kcal/mol). Among the isomers arising from the terminations of radical anions **24** and **21**, Table 6 also shows that their stabilities could be roughly divided into three categories: the lithium alkyl dicarbonates with a long chain, **33** [$(CH{=}CHOCO_2Li)_2$ solvated by EC], **35** ($LiO_2COCH{=}CHCH_2CH_2OCO_2Li$, two tails solvated by EC and VC, respectively), and **27** [$(CH_2CH_2OCO_2Li)_2$ solvated by VC], have the lowest relative Gibbs free energies (−140.6, −138.1, and −136.7 kcal/mol), followed by the lithium alkyl dicarbonates with a short chain and/or lithium carbonate, **26** [$(CH_2OCO_2Li)_2$ solvated by VC + ethylene gas, −128.0 kcal/mol] ∼**31** [$(CHOCO_2Li)_2$ solvated by VC and EC in the two respective tails + ethylene gas, −127.5 kcal/mol] < **30** [Li_2CO_3 solvated by two VC and one EC + ethylene gas, −125.0 kcal/mol] < **34** [$(CHOCO_2Li)_2$ solvated by EC + acetylene gas, −121.3 kcal/mol] < **29** [$LiO(CH)_2CO_2(CH_2)_2OCO_2Li$ solvated by EC and VC in the two tails, −118.9 kcal/mol], and the C−Li carbides **36** and **28** have the highest ΔG (−106.4 and −103.1 kcal/mol).

D. More Realistic Models for Solvent Effects. $(EC)_2Li^+$(VC) and $(EC)_3Li^+$(VC). To incorporate the fact that only small amounts of VC are added in lithium-ion electrolyte, the electroreductive decompositions are further investigated for two more realistic clusters, $(EC)_2Li^+(VC)$ (**37**) and $(EC)_3Li^+(VC)$ (**45**). Energetic data and other characteristics are collected in Table 8, and their profiles of the potential energy surface and Gibbs free energy surface are shown in Figures 7 and 8, respectively. Li^+ coordinates with O1 (carbonyl oxygen) as well as one of O2 (ethereal oxygen) of the reduced EC/VC molecule in the reduction intermediates of $Li^+(VC)$ and $(EC)Li^+(VC)$, where the distances are 1.802/1.879 Å (1.883/2.106 Å in bulk solvent) for **6**, 1.832/1.912 Å for **16**, and 1.832/1.955 Å for **17**. Yet Li^+ moves far away from O2 (beyond 3 Å); thus it only coordinates with O1 in the $(EC)_2Li^+(VC)$ and $(EC)_3Li^+(VC)$ reduction intermediates perhaps due to more $Li^+{\cdots}O{=}C$ interactions. Qualitatively in line with the PCM-optimization result performed for $Li^+(VC)$, another clear effect of the solvent molecules on the reduction intermediate is that the C (carbonyl carbon)−O2 bonds are not yet as loose as those in **6**, **16**, and **17**; for example, the C−O2 bond lengths are 1.606 (**6**), 1.559 (**16**), 1.567 (**17**), 1.468 (**38**), 1.433 (**39**), 1.473 (**46**), and 1.465 Å(**47**).

The reductive decompositions of **37** and **45** are similar to that of **15** from a mechanistic viewpoint; however, their adiabatic *EA*s are decreased further (70.1 and 64.0 kcal/mol for VC- and EC-reduction in **37**, 64.1 and 58.8 kcal/mol for **45**) by the explicit inclusions of one and two more EC molecules, and the energy released by the radical anion formation is also decreased (−81.4, −77.0 vs −91.8 kcal/mol for VC ring opening, −92.2, −85.4 vs −104.2 kcal/mol for EC ring opening). The VC-reduction intermediates, **38** and **46**, get extra stability from the coordinated EC molecules; for example, they have 6.1 and 5.3 kcal/mol less energy than do EC-reduction intermediates, **39** and **47**, respectively. This result is a strong indication that VC

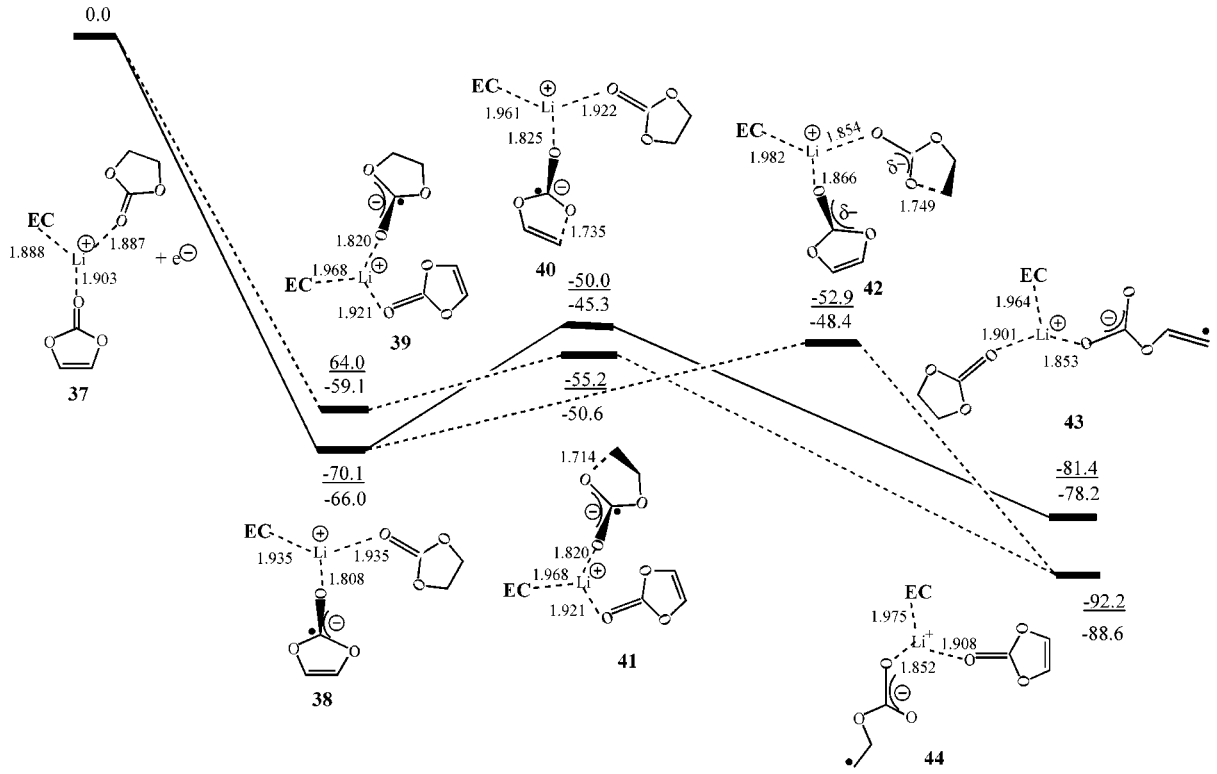

Figure 7. Potential energy (underlined data) and Gibbs free energy profile at 298.15 K for the reductive decomposition process of $(EC)_2Li^+(VC)$ calculated with the B3PW91/6-311++G(d,p)// B3PW91/6-31G(d) method.

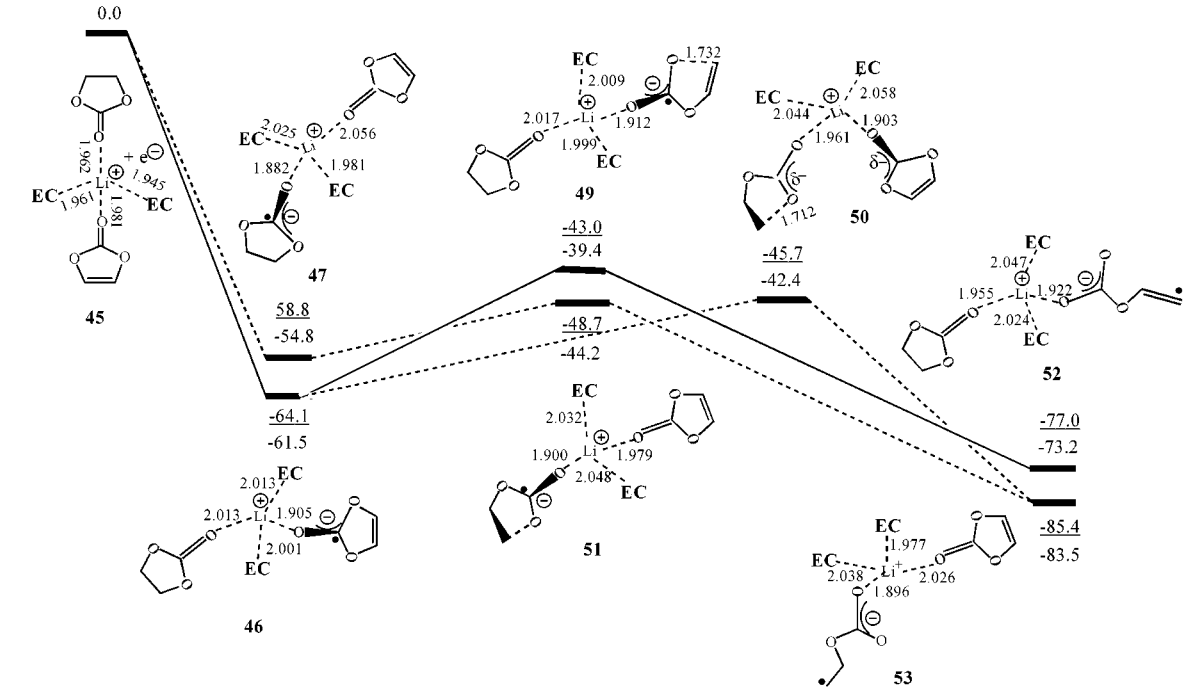

Figure 8. Potential energy (underlined data) and Gibbs free energy profile at 298.15 K for the reductive decomposition process of $(EC)_3Li^+(VC)$ calculated with the B3PW91/6-311++G(d,p)// B3PW91/6-31G(d) method.

is more easily reduced than the EC molecule in the EC-based Li-ion battery electrolyte where VC is used as an additive. Regarding the ring-opening reactions, like the preceding results predicted by the CPCM approach for the cluster $(EC)Li^+(VC)$, the energy barriers for the EC-reduction intermediates, **39** and **47**, are slightly decreased via transition states, **41** and **51**, as compared with those of **15** (8.8, 10.1 vs 11.2 kcal/mol), which is probably induced by more charge separation of the carbonyl group. In the cases of the VC-reduction intermediates, **38** and **46**, both the transition states of the VC ring openings, **40** and **49**, and those corresponding to the EC-moiety, **42** and **50**, are also identified. The ring-opening barriers for VC remain close to that of **16** (20.1, 21.1 vs 20.4 kcal/mol), whereas the inclusions of one and two more EC molecules considerably

increase those for the EC moiety by 4−5 kcal/mol (17.2, 18.4 vs 13.5 kcal/mol), which are in line with those predicted by (EC)Li^+(VC)-CPCM for the path (17.8 and 13.5 kcal/mol after and before CPCM correction). Several termination reactions of radicals **43** and **44** generating lithium alkyl dicarbonates are evaluated, which are equivalent to paths A and B in Figure 6b, and to paths A, E, and F in Figure 6c. Except for the extra EC/VC solvent coordinated with the Li^+ at each end, the structures of these lithium alkyl dicarbonates are rather similar to their analogues in Figure 6b and c. Generally, the ΔGs are more negative by only a few kcal/mol than those in the case of (EC)Li^+(VC); for example, ΔGs for the three paths corresponding to the A, E, and F in Figure 6c are −101.6, −83.2, and −63.2 kcal/mol (vs −99.0, −81.1, and −59.9), respectively.

E. Brief Remarks on the Factors Relevant to the Additive Role of VC. Reductive Decomposition Mechanisms. On the basis of the above investigation, the possible roles of VC as an additive in EC-based solvent of lithium-ion batteries could be explained by introducing four alternative reduction schemes.

Scheme A. VC Reductive Decomposition. Because the VC molecule in the model (EC)Li^+(VC) is more easily reduced than EC by approximately 5.0 kcal/mol, VC is initially reduced to the more stable intermediate releasing quite a large amount of energy (about 40 kcal/mol). VC then undergoes decompositions via a higher barrier (about 20 kcal/mol) as compared with EC; for example, **45** + e^- → **46** → TS, **49** → **52** as shown in Figure 8. We suggest that determining the amount of VC lost upon the SEI formation could test this pathway. Such a study has not been reported yet.

Scheme B. EC Reductive Decomposition. Because of its low energy barrier (10 ± 1.0 kcal/mol), EC will be initially reduced to an ion-pair intermediate and then undergo a homolytic C−O bond cleavage, that is, **45** + e^- → **47** → TS, **51** → **53**. Although this pathway is kinetically favorable, the effect of VC is unclear; for example, as shown in Table 9, the *EA* of (EC)Li^+(VC) corresponding to the EC reduction is only 1.9 kcal/mol higher than that of $Li^+(EC)_2$. However, they are nearly identical in the more practical cases of $(EC)_3Li^+$(VC) and Li^+-$(EC)_4$ (58.8 vs 59.0 kcal/mol, see Table 9).

Scheme C. VC Catalyzes the Decomposition of EC. (EC)-Li^+(VC) is initially reduced to the most stable ion-pair intermediate **46** by VC reduction, and then a homolytic ring opening will take place on the EC moiety instead of being on the reduced VC, via an intramolecular electron-transfer TS **50**, generating the more stable radical anion **53**, that is, **45** + e^- → **46** → TS, **50** → **53**. The energy barrier is lower than that given in scheme A, although it is still higher than that in scheme B.

Scheme D. VC Initiates the Decomposition of EC. The suggested mechanism is that VC is initially reduced to an ion-pair intermediate, and then the intermediate will nucleophilicly attack the EC molecule of the supermolecule, resulting in EC decomposition, that is, **45** + e^- → **46**, **46** + **45**. Upon electron transfer from the reduced VC molecule, EC decomposes. The scheme is under investigation. According to schemes C and D, VC will not be consumed; therefore it could be thought of as a catalyst. In principle, all the schemes except B could contribute individually and in a parallel manner to the role that VC plays as additive.

Solvation and Reduction Potential. The solvation of Li^+ is easier in EC than in VC, which is reflected by the shorter O−Li^+ distances in (EC)Li^+(VC), 1.813 vs 1.825 Å, as shown in Figure 6a, 1.888 vs 1.903 Å in the model **37** shown in Figure 7, as well as by the binding energies of Li^+ with each of the solvents (48.0 and 44.0 kcal/mol for EC and VC, respectively, at B3PW91/6-311++G(d,p) with ZPE correction). The AIM result is another indication of the VC's weak solvation ability toward Li^+: $\rho(r) = 0.032$ au, $\nabla^2\rho(r) = 0.289$ at the bcp between Li^+ and the VC carbonyl oxygen, and $\rho(r) = 0.034$ au, $\nabla^2\rho(r) = 0.303$ at the bcp between Li^+ and the EC carbonyl oxygen. Taking into account the fact that VC could play the role of an additive in EC, PC, or their mixtures, these results imply that a strong solvation perhaps is not a critical factor for a compound to be an efficient additive. On the other hand, the VC-reduction intermediate (**17**) is more stable than the EC-reduction intermediate (**16**) by 3.1 kcal/mol in the gas phase and by 6.2 kcal/mol in solution. Therefore, the reduction potential corresponding to the ion-pair intermediate formation may be an important index to evaluate a lithium-ion battery electrolyte additive candidate.

Regarding the Products from VC and EC Reduction. The major components for both EC and VC are organic products, such as lithium dicarbonates with one and two alkyl units, $(ROCO_2Li)_2$ and $(R_2OCO_2Li)_2$ (R═CH,CH_2 for VC and EC, respectively), $LiOROCO_2Li$, and lithium carbide (LiR_2OCO_2Li) compounds with an Li−C bond. The difference is that $(R_2OCO_2Li)_2$ and lithium carbide in the case of VC are likely to be in higher proportion than in the case of EC, whereas $(ROCO_2Li)_2$ is expected to be found in higher concentrations in EC than in VC. Although our preliminary studies on the adsorption of the lithium dicarbonates on the surface of graphite do not reveal a significant difference with respect to the graphite−dicarbonate interaction energy both between $(ROCO_2Li)_2$ and $(R_2OCO_2Li)_2$ and between the lithium dicarbonates with R = CH and CH_2,[28] the fact that VC reduction products contain double bonds may be responsible for the improvement over the SEI film formation. One possible mechanism is that unsaturated lithium dicarbonates could be further polymerized on the electrode's surface, thus forming polymeric surface films that improve the passivation of the anode. Oligomers with repeated vinylene as well as carbonate-vinylene units could be generated when VC is present in the electrolyte, via radical anion (**8**) attacking the double bond of VC and via carbon anion (**10**) nucleophilicly attacking the carbonyl carbon of VC, respectively, which may also contribute to the role which VC plays as an EC-based electrolyte additive.

In brief, for a substance to behave as a proper additive of lithium-ion battery electrolyte with a primary function of contributing to the SEI formation, the ideal candidate at least should have higher negative reduction potential than the supporting solvents such as EC, PC, and EC/DMC, so that it could be reduced well before the supporting solvent, and it is also necessary that the final reduction products could form a more effective SEI film. The present study presents a procedure for additive selection. The procedure involves ab initio calculations that provide energetic data for alternative paths. The outcome of the procedure also clearly determines which experiments are needed to obtain quantitative and definite information about the additive role.

(28) H-truncated carbon cluster ($C_{54}H_{18}$) was used to model graphite surface. The binding energies of $(CH_2OCO_2Li)_2$, $(CH_2CH_2OCO_2Li)_2$, $(CHOCO_2Li)_2$, and $(CHCHOCO_2Li)_2$ are 40.5, 38.7, 38.3, and 35.4 kcal/mol, respectively, at PW91PW91/3-21G level.

Conclusions

High-level density functional calculations have been carried out for an isolated VC, and for supermolecules such as $(EC)_nLi^+$-(VC) ($n = 0-3$)[29] to elucidate the role of VC as an electrolyte additive of lithium-ion battery. For the solvated VC, the solvent effect considerably stabilizes the reduction intermediate, the relative energies of which are further decreased by 5.0 kcal/mol or so due to the salt effect. The electron affinities of $(EC)_nLi^+(VC)$ ($n = 0-3$) monotonically decrease with the explicit inclusion of more solvent molecules; initially it decreases sharply about 20.0 kcal/mol from $n = 0$ to 1 and then by a gentle variation. In the cases of the supermolecules $(EC)_n(VC)Li^+$ ($n = 1-3$), the VC reduction brings about more stable ion-pair intermediates than those of the EC molecule by 3.1, 6.1, and 5.3 kcal/mol, respectively, which qualitatively agrees with the experimental fact that the reduction potential of VC in the presence of Li salt is lower than that of EC. Numerically, the reduction potentials corresponding to radical anion formations (electrochemical reactions IV and VI), predicted with the cluster-continuum model $(EC)Li^+(VC)$-CPCM, are close to the experimental potentials on the gold electrode surface (-2.67, -3.19 eV on the physical scale for VC and EC, respectively, vs -2.96 and -2.94 eV[22]). The predicted reduction potentials from the cluster $(EC)_3Li^+(VC)$ model are about 10.0 kcal/mol higher than those from $(EC)Li^+(VC)$-CPCM; therefore a cluster-continuum hybrid model is necessary to describe both specific and bulk solvent effects.

Regarding the ring-opening mechanism of the EC- and VC-reduction intermediates, the energy barrier for the reduced-VC homolytic ring opening is about one time higher than that of reduced EC (e.g., 20.4 vs 11.1 kcal/mol for $(VC)Li^+(EC)$). Solvent effects on them are very weak as indicated by explicit inclusion of EC molecules as well as by further polarized continuum model calculations. Starting from the VC-reduction intermediate of the supermolecule $(VC)Li^+(EC)$, another decomposition path has also been found; that is, the ring opening occurs on an unreduced EC instead of on the reduced VC molecule. The energy barrier for homolytic ring opening for EC is 13.5 kcal/mol, which is 6.9 kcal/mol lower than that of the reduced VC and only 2.4 kcal/mol higher than that of the reduced EC yielding another less stable ion-pair intermediate. Although in the kinetic aspect the channel is not as favorable as in the case of $(EC)Li^+(VC)$, the result is also qualitatively supported by the complex models of $(EC)_nLi^+(VC)$ ($n = 2$ to 3) as well as the $(EC)Li^+(VC)$-CPCM hybrid model calculation.

The role of VC as an additive in EC-based solvent of lithium-ion batteries may be explained in the following manners: once a carbon anode is polarized to low potentials in an organic polar aprotic solution containing lithium salts ($EC/VC/Li^+$), VC is initially reduced to a more stable intermediate than that from EC reduction, releasing quite a large amount of energy (about 40 kcal/mol). With this energy release, then the reduced VC may undergo a decomposition to form a radical anion via a barrier of about 20 kcal/mol. The products (lithium alkyl dicarbonate, R−O−Li compound, Li−C carbides, oligomers with repeated vinylene and carbonate-vinylene units) from the termination reactions of the radical anion would build up an effective SEI film. Compared with the reduction products of EC, the VC reduction products contain double bonds that may be responsible for the improvement over the SEI film formation by further polymerizing on the electrode's surface. Thus, the products initiated by VC reduction could form an effective SEI film well before the reduction of the supporting solvent EC/PC so as to prevent the massive reduction of supporting solvent. As EC is used as supporting solvent, VC may simultaneously play its additive role in another way; that is, starting from the VC-reduction intermediate, the ring opening occurs on the unreduced EC moiety instead of being on the reduced VC, via an intramolecular electron-transfer TS, the energy barrier of which is lower than that of the VC ring opening.

Acknowledgment. This work was partially supported by NSF (Career Award grant CTS-9876065 to P.B.B.), by Mitsubishi Chemical Corp., and by DOE Cooperative Agreement DE-FC02-91ER75666. We acknowledge supercomputer resources provided by the National Computational Science Alliance under grants CHE000040N, CTS000016N, CTS00007N (Y.W., P.B.B.) and by NERSC.

JA017073I

(29) Upon request, coordinates of the optimized structure will be provided.
(30) Private communication with Nakamura, S.; Ue, M. (MCC, Japan).